Inorganic Chemistry

Article

pubs.acs.org/IC

Synthesis, Characterization, and DFT Analysis of Bis-Terpyridyl-Based Molecular Cobalt Complexes

Safwan Aroua,[†] Tanya K. Todorova,[†] Paul Hommes,[‡] Lise-Marie Chamoreau,[§] Hans-Ulrich Reissig,[‡] Victor Mougel,[†] and Marc Fontecave*[,†]

[†]Laboratoire de Chimie des Processus Biologiques, UMR 8229 CNRS, Collège de France, Université Paris 6, 11 Place Marcelin Berthelot, 75231 Paris Cedex 05, France

[‡]Institut für Chemie und Biochemie, Freie Universität Berlin, Takustrasse 3, 14195 Berlin, Germany

[§]Sorbonne Universités, UPMC Université Paris 6, Institut Parisien de Chimie Moléculaire, UMR 8232 CNRS, 4 Place Jussieu, 75252 Paris Cedex 5, France

Supporting Information

ABSTRACT: Terpyridine ligands are widely used in chemistry and material sciences owing to their ability to form stable molecular complexes with a large variety of metal ions. In that context, variations of the substituents on the terpyridine ligand allow modulation of the material properties. Applying the Stille cross-coupling reaction, we prepared with good yields a new series of terpyridine ligands possessing quinoline-type moieties in ortho, meta, and para positions and dimethylamino substituents at central or distal positions. The corresponding cobalt(II) complexes were synthesized and fully characterized by elemental analysis, single-crystal X-ray crystallography, mass spectrometry, and UV−vis, ^{1}H NMR, and Fourier transform infrared (FT-IR) spectroscopy as well as by cyclic voltammetry (CV). Density functional theory (DFT) calculations were performed to investigate the electronic structure of all the Co(II) bis-terpyridyl molecular complexes. In this work, we show that terpyridine ligand functionalization allows tuning the redox potentials of the Co(III)/Co(II), Co(II)/Co(I), and Co(I)/Co(I)(tpy)$^{\bullet-}$ couples over a 1 V range.

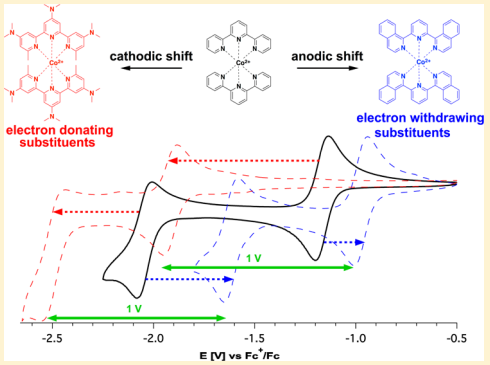

INTRODUCTION

Molecular complexes containing a metal center and one or two terpyridine ligands have been extensively studied not only as photosensitizers,[1] redox shuttles for dye-sensitized solar cells (DSSC),[2] anolytes for redox flow batteries,[3] ion sensors,[4] nanowire transistors,[5] and supramolecular polymers[6] but also for nonlinear optics[7] and catalysis for proton[8] and CO_2 reduction.[8a,9] The properties of such complexes have been shown to be strongly influenced by the electronic nature of the terpyridine ligands. The potential applications of terpyridyl complexes as photosensitizers have been previously investigated by Damrauer and co-workers, using an iron complex, and by Berlinguette and co-workers, using ruthenium complexes.[1] Limitations arise from the lack of efficient procedures to synthesize new terpyridine ligands, in particular those bearing electronically different substituents, which is still a current research topic.[10]

Following the initial synthesis of terpyridine in 1932 by oxidative coupling of pyridine using anhydrous $FeCl_3$ salt,[11] several alternative synthetic routes have been employed; however, these have met with limited efficiency in terms of yield and selectivity. Syntheses based on Pd(0)-catalyzed pyridine coupling[12] or oxidation of diacetylpyridine, followed by a condensation with an α,β-unsaturated aldehyde in the presence of ammonium acetate,[13] have been proposed. Such methods and other similar ones allowed the introduction of aliphatic functional groups.

Syntheses using Hiyama, Suzuki, and Stille cross-coupling reactions have recently been reported.[14] In particular, the application of Stille cross-coupling for the preparation of terpyridines achieved in 1996 by Sauvage and co-workers[14c] allowed the isolation of a variety of substituted terpyridines. Surprisingly little has been done to study the electronic effects of these ligands on the physicochemical properties of their metal complexes.[8a]

In this work, we have studied the new series of substituted terpyridine ligands **L2**−**L8**, shown in Figure 1, with the parent terpyridine ligand **L1** as a reference. The introduced functional groups were chosen to allow investigating the influence of a broad range of electronic environments. Ligand **L2** holds two highly antagonistic electronic groups: one electron-donating substituent (dimethylamino) on the central ring and two electron-withdrawing substituents (trifluoromethyl) on the distal rings. **L2** was chosen to investigate the influence of functionalization at the 4-distal position relative to the 4-central

Received: March 6, 2017

DOI: 10.1021/acs.inorgchem.7b00595
Inorg. Chem. XXXX, XXX, XXX−XXX

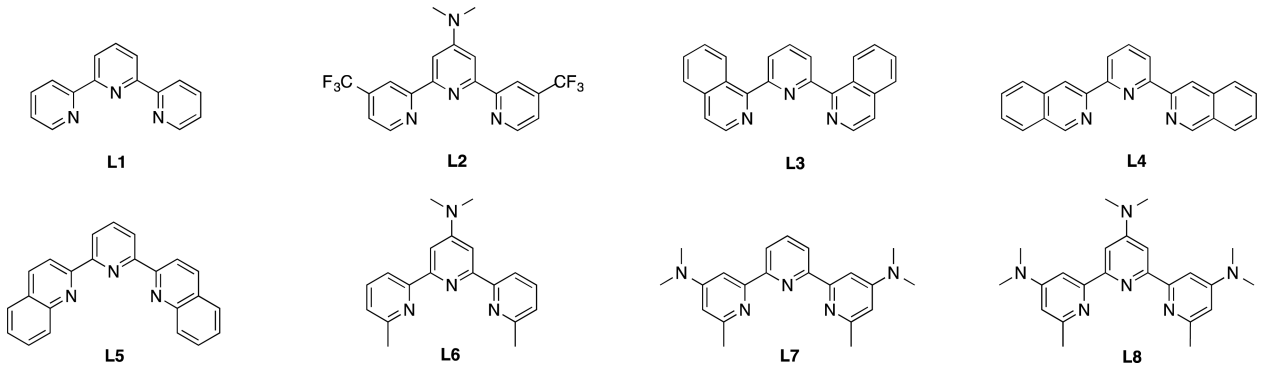

Figure 1. New terpyridine-based ligands prepared in this study (**L1** is used as a reference).

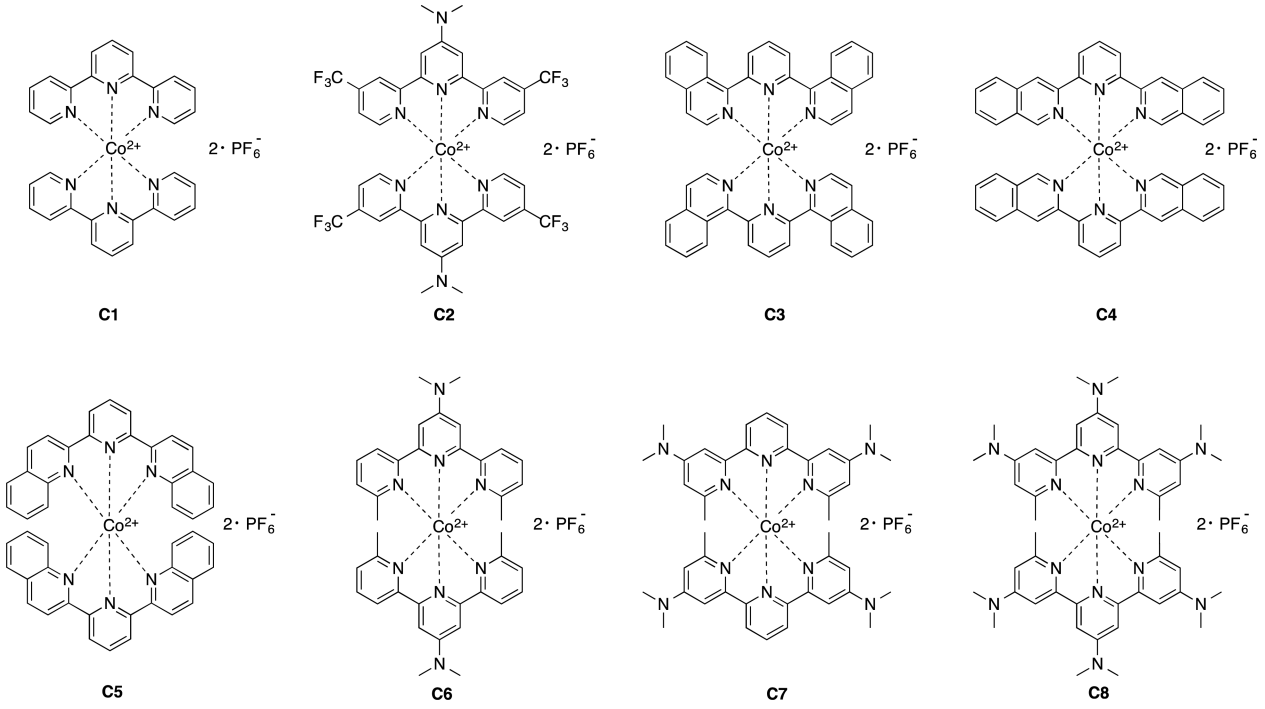

Figure 2. Cobalt bis-terpyridyl-based molecular complexes (**C1**–**C8**) investigated in this work.

position, with special interest in compensating effects. Ligands **L3**–**L5** holding quinolines in three different orientations (**L3**, ortho; **L4**, meta; **L5**, para) were designed as compounds with the potential ability to delocalize a negative charge. Ligands **L6**–**L8** form a class of strongly electron enriched dimethylamino-based terpyridines. The number of 4-dimethylamino groups varied from one on the central ring in **L6** to two on distal rings in **L7** or one on each ring in **L8**. In addition, ligands **L6**–**L8** possess a methyl group at the 2-position acting as a weak electron donor.

The corresponding cobalt(II) bis-terpyridyl molecular complexes **C1**–**C8** (Figure 2) were prepared and characterized by single-crystal X-ray diffraction, ^{1}H NMR, FT-IR and UV–vis spectroscopy, mass spectrometry, and cyclic voltammetry, as well as by DFT computations. This provides a means to determine the influence of the electronic effects of the terpyridine substituents on the physicochemical properties of the complexes.

RESULTS AND DISCUSSION

Synthesis of Substituted Terpyridine Ligands. Synthesis of the ligands using Hiyama, Negishi, and Suzuki cross-coupling reactions proved unsuccessful, affording only traces of products. The various reaction conditions investigated are summarized in Scheme S3 in the Supporting Information. Alternatively, we investigated a synthetic route based on the Stille cross-coupling reaction, as described in Figure 3. Two different strategies were followed: (i) for the preparation of quinoline derivatives (**L3**–**L5**), 2-halopyridine **1** was coupled to 2,6-bis(organostannyl)pyridine **2**; (ii) for terpyridines having a dimethylamino group on the central ring (**L2**, **L6**), 2-(organostannyl)pyridine **3** was coupled to 2,6-diiodopyridine **4** (Figure 3). Both strategies provided sufficient amounts of product, with isolated yields of 37–94%. Ligands **L7** and **L8** having distal dimethylamino groups were prepared according to previously reported procedures involving the coupling of 2,6-pyridinedicarboxylic acid derivatives **5** with β-ketoenamine **6** and a subsequent cyclocondensation reaction to **7** followed by activation and aromatic nucleophilic substitution.[15]

DOI: 10.1021/acs.inorgchem.7b00595
Inorg. Chem. XXXX, XXX, XXX–XXX

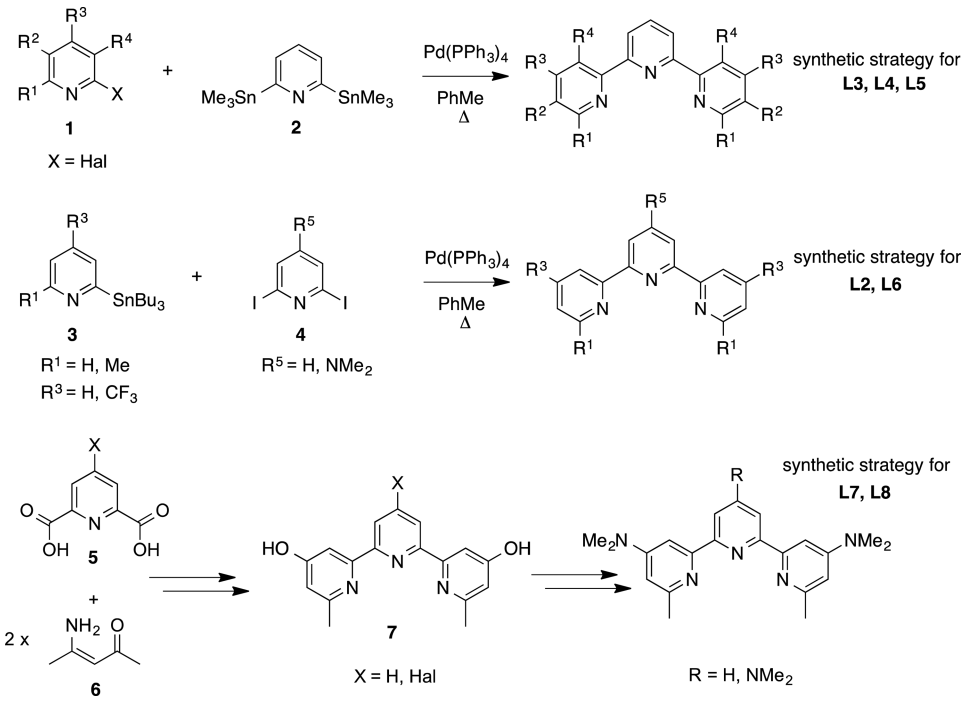

Figure 3. Synthetic strategies applied to obtain ligands **L2**−**L8**.

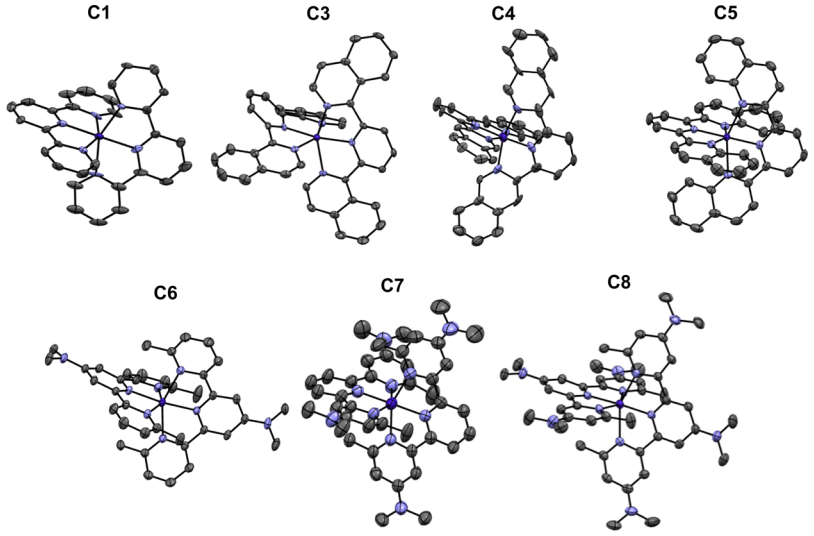

Figure 4. Crystal structures of molecular complexes **C1** and **C3**−**C8**. Hexafluorophosphate counterions, hydrogen atoms, and solvent molecules were omitted for clarity (ellipsoid representations at the 50% probability level).

Synthesis of $[Co(terpyridyl)_2](PF_6)_2$ Complexes. The corresponding bis-substituted cobalt(II) complexes **C1**−**C8** were obtained by reacting stoichiometric ratios of the ligand and cobalt dichloride in methanol under reflux followed by precipitation of the complex through anion exchange with ammonium hexafluorophosphate (NH_4PF_6).[16] All complexes are paramagnetic, as confirmed by their ^{1}H NMR spectra showing peaks at up to ca. 120 ppm (Figures S12−S19 in the Supporting Information). For all complexes the number of peaks in proton NMR at 300 K is consistent with a C_{2v} symmetry. The bands assigned to the ligands in the FT-IR spectra of complexes **C1**−**C8** are characterized by significant shifts reflecting complexation with cobalt(II) (Figure S49 in the Supporting Information). The electronic effects of the ligands can be probed by UV−vis spectroscopy: (i) the π−π^* transition bands (allowed transitions) in the UV−vis spectra are red-shifted upon complexation with Co(II) (e.g., λ_{max}(**L1**) 277 nm and λ_{max}(**C1**) 317 nm, Figures S50−S57 in the Supporting Information) and (ii) light absorption by complexes **C1**−**C8** starts at much lower energy (ca. 500−600 nm), in comparison to the free ligands (below 400 nm) (Figures S50−S57).

Crystal Structures. Crystals were obtained by slow evaporation of acetone/toluene (2/1 v/v) solutions of the complexes. The crystal structures were determined for **C1** and **C3**−**C8** (single crystals of **C2** of sufficient quality could not be obtained) and are shown in Figure 4 (crystallographic parameters are given in Tables S1 and S2 in the Supporting Information). Distorted-octahedral geometries (ML_6) were found for all complexes, with two ligands per Co center and

DOI: 10.1021/acs.inorgchem.7b00595
Inorg. Chem. XXXX, XXX, XXX−XXX

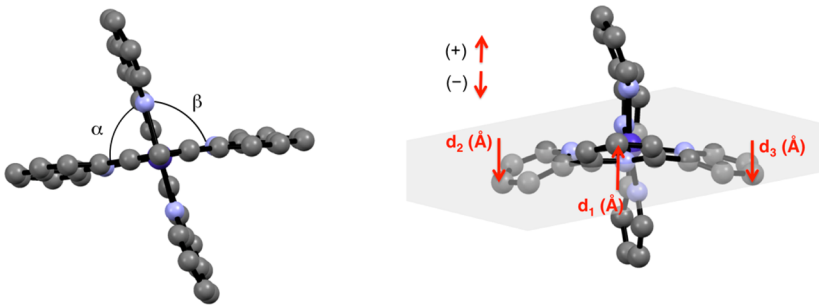

Figure 5. (a) Deviation from orthogonality descriptors: acute angle α and obtuse angle β (averaged N_{dist}−Co−N_{dist} angles). (b) Deviation from planarity descriptors d_1, d_2, and d_3 (the three N atoms of the ligand define a plane). Arbitrarily, the central ring is always defined above the plane. Deviations above or below the plane are denoted with + and −, respectively.

Table 1. Descriptors for the Deviation from Orthogonality (α and β in deg) and for the Deviation from Planarity (d_1, d_2, and d_3 in Å)[a]

			C1	C2	C3	C4	C5	C6	C7	C8
exptl (standard deviation)		α (av)	93.15		91.3	90.3	89.3	91.0	92.1	92.4
		β (av)	93.59		96.0	92.6	97.3	95.8	94.5	94.5
		d_1 (av)	+0.00(6)		+1.14(8)	+0.2(1)	+0.0(0)	+0.13(0)	+0.3(2)	+0.2(2)
		d_2 (av)	−0.07(6)		−0.7(4)	−0.16(2)	+0.39(4)	−0.75(0)	−0.5(3)	−0.0(1)
		d_3 (av)	−0.1(2)		−0.62(1)	+0.3(5)	−0.39(4)	+0.18(0)	+0.0(4)	−0.04(3)
DFT	doublet	α (av)	91.7	91.7	91.9	91.6	81.1 (89.7)	89.8	90.6	90.5
		β (av)	91.7	92	92	91.6	103.5 (94.5)	94.6	93.5	93.9
		d_1 (av)	0.0	+0.01	+0.88	+0.01	0.0 (+0.02)	0.0	0.0	0.0
		d_2 (av)	0.0	+0.01	−0.41	+0.01	−1.23 (+0.51)	+0.62	+0.58	+0.63
		d_3 (av)	0.0	+0.01	−0.37	−0.01	+1.23 (−0.70)	−0.62	−0.60	−0.65
	quartet	α (av)	94	90.3	92.7	93.8	85.2 (91.3)	90.8	91.9	91.9
		β (av)	94	97	95	93.9	104 (97.4)	97.2	96.2	96.3
		d_1 (av)	+0.02	+0.02	+1.30	+0.01	+0.46 (+0.21)	+0.31	+0.29	+0.38
		d_2 (av)	+0.01	−0.08	−0.36	+0.04	−1.01 (+0.58)	+0.33	+0.30	+0.24
		d_3 (av)	+0.01	+0.09	−0.40	+0.04	+1.13 (−0.61)	−0.80	−0.64	−0.73

[a]Experimental and corresponding computed values (M06-L/6-311+G(d,p) level of theory, 0 K) for both low-spin doublet and high-spin quartet spin states of complexes **C1**−**C8** are reported. For **C5**, the computed values in parentheses were obtained from an optimized structure with four toluene solvent molecules (see Figure S75 in the Supporting Information).

Table 2. Average Co−Central Nitrogen or Co−Distal Nitrogen Bond Lengths (Å) in the Crystal Structures and the Corresponding Computed Bond Lengths (M06-L/6-311+G(d,p) Level of Theory, 0 K) for both Low-Spin Doublet and High-Spin Quartet Spin States of Complexes C1−C8[a]

	exptl (standard deviation)		DFT			
			doublet		quartet	
	Co−N_{cent} (av)	Co−N_{dist} (av)	Co−N_{cent} (av)	Co−N_{dist} (av)	Co−N_{cent} (av)	Co−N_{dist} (av)
C1 (100 K)	2.05(3)	2.17(2)	1.898	2.109	**2.089**	2.185
C2			1.901	2.111	2.068	2.187
C3 (100 K)	2.06(1)	2.15(1)	1.925	2.091	**2.101**	2.167
C4 (100 K)	1.88(3)	2.06(6)	**1.898**	2.105	2.090	2.179
C5 (200 K)	2.04(1)	2.272(1)	1.899	2.187	**2.081**	2.262
C6 (200 K)	2.02(0)	2.27(8)	1.905	2.199	**2.058**	2.280
C7 (200 K)	2.046(5)	2.22(2)	1.904	2.182	**2.090**	2.248
C8 (200 K)	2.043(3)	2.23(3)	1.906	2.185	**2.073**	2.257

[a]Values in boldface are the computed Co−central nitrogen distances in agreement with the measured values.

three nitrogen atoms of each ligand coordinating the cobalt(II) ion. For each complex, two hexafluorophosphate counterions are present in the unit cell to balance the charges.

We first examined the structural changes induced by the different substituents on the ligands. We defined the orthogonality between the ligands in each complex by means of two parameters: the acute α and the obtuse β N_{dist}−Co−N_{dist} angles as shown in Figure 5a. A difference between these two values reflects a deviation from orthogonality. The results are summarized in Table 1. While in complex **C1**, as well as in **C4**, **C7**, and **C8**, the angles α and β have comparable values with differences <3°, significant deviations are observed in the case of complexes **C3**, **C5**, and **C6** (Table 1), with α and β values of 89 and 97°, respectively (**C5**), and 91 and 96°, respectively (**C3** and **C6**). The largest deviation was observed for complex **C5**, likely due to intermolecular π−π interactions with neighboring

DOI: 10.1021/acs.inorgchem.7b00595
Inorg. Chem. XXXX, XXX, XXX−XXX

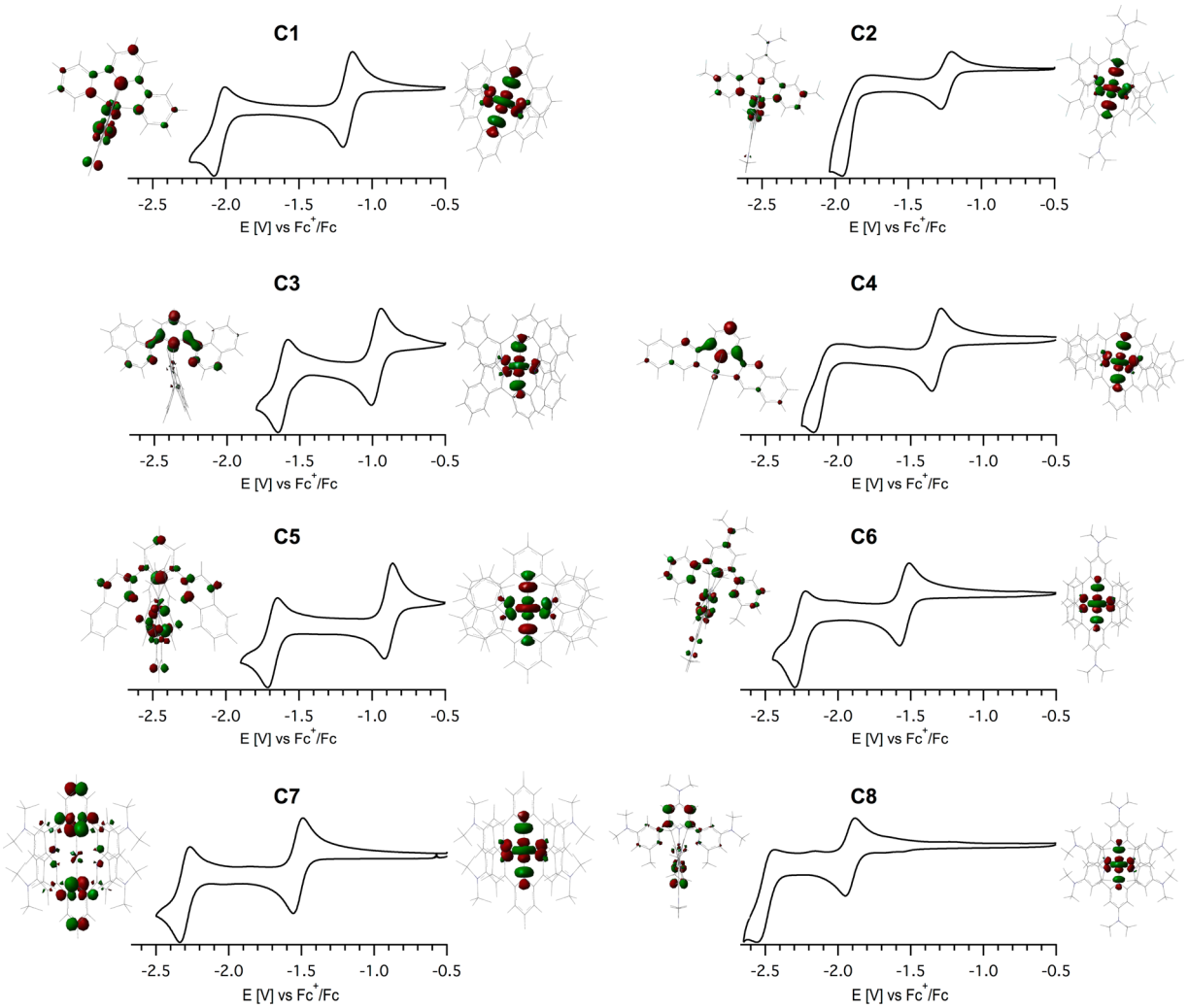

Figure 6. Cyclic voltammetry experiments of **C1**−**C8** (1.0 mM) in acetonitrile as solvent with tetrabutylammonium perchlorate supporting electrolyte (0.1 M). The scan rate was 50 mV/s (the first two reductions were measured). The molecular orbitals on which the electrons reside for each of the two one-electron-reduction events are depicted for each complex.

complexes and cocrystallized toluene solvent molecules (see below).

Additionally, deviation from planarity of the ligands in these complexes was quantified using the three descriptors d_1, d_2, and d_3 (see Figure 5b): they account for the deviation of each pyridyl ring with respect to a plane defined by the three nitrogen atoms of one ligand. The descriptors measure the corresponding distance between the plane and the 4-pyridyl position in each pyridyl ring (see Table 1).

The ligands in **C1** are fully planar (<0.07 Å deviation), while those in **C8** deviate slightly from ideal planarity (d_1 is only +0.2 Å). Ligands in **C3** show the largest deviation, which likely originates from the steric repulsion of hydrogens from central and distal 3-pyridyl positions. As a result, the central pyridyl ring is displaced upward (d_1 = +1.14 Å) and the distal rings are displaced downward (d_2 = −0.70 Å, d_3 = −0.62 Å). In contrast, ligands in **C4**−**C7** have a distorted shape, with a d_2 value as high as 0.75 Å in **C6**. It seems that planarity is obtained when the three pyridyl moieties of the ligand are identical, while significant distortions occur when they differ in their substituents.

Table 2 reveals that the bond lengths between the cobalt ion and the central nitrogen (Co−N_{cent}) are 0.09−0.25 Å shorter than the distances between the cobalt ion and the distal nitrogen (Co−N_{dist}). Surprisingly, the Co−N_{cent} distance in complex **C4** is significantly shorter (1.88 Å) than the corresponding Co−N_{cent} distances in the other complexes that vary in the range of 2.02−2.06 Å. The Co−N_{dist} bond lengths in that complex (2.06 Å) are also significantly shorter than the Co−N_{dist} distances in the other complexes (2.15−2.27 Å). Since the redox state of these systems is the same, it is likely that the uniqueness of **C4** is due to adoption of a different spin state (see below).

The steric bulk of the ligands was measured using the V_{Bur} (% buried volume) parameter defined as the fraction of the total volume of a sphere, centered on the metal, occupied by the ligand, using the crystallographic data (see Figure S58, in the Supporting Information for details).[17] For the calculations, the sphere radius was chosen as the distance between the cobalt center and the centroid of the two carbon atoms adjacent to the central N atom. That distance in **C1** is 2.7 Å and was used as a reference. The radius R and the mesh spacing were fixed to 3.5 and 0.05 Å, respectively. Consequently, the ligands **L1**−**L8** could be divided into two classes in terms of steric hindrance (Table S3 in the Supporting Information): **L1**−**L4** define the first class, occupying a low buried volume between 15.5 and

DOI: 10.1021/acs.inorgchem.7b00595
Inorg. Chem. XXXX, XXX, XXX−XXX

Table 3. Measured Reduction Potential ($V/Fc^{0/+}$) of C1−C8 in 0.1 M $TBAClO_4$ Electrolyte Solution in CH_3CN and Oxidation Potential in 0.1 M LiTFSI Electrolyte Solution in CH_3CN[a]

	C1	C2	C3	C4	C5	C6	C7	C8
E^{ox1}	−0.07	−0.04	−0.09	−0.21	+0.84	+0.53	+0.25	+0.03
E^{red1}	−1.17	−1.24	−0.82	−1.32	−0.89	−1.54	−1.52	−1.92
E^{red2}	−2.04	−1.91	−1.61	−2.13	−1.68	−2.26	−2.30	−2.49

[a]See the Supporting Information for details. E^{ox1} is the first oxidation of $[Co(bis\text{-}terpyridyl)]^{2+}$ and E^{red1} and E^{red2} are the first and second one-electron reductions of $[Co(bis\text{-}terpyridyl)]^{2+}$, respectively.

19.0%, while **L5**−**L8** define a second class, with a larger buried volume of 24.5−26.5%. Such significant differences are attributed to the presence of a methyl- or aryl-type carbon on the 2-position of the distal pyridyl ring.

Cyclic Voltammetry. In order to investigate the influence of the terpyridine substituents on the redox properties of the complexes, cyclic voltammograms (CVs) of complexes **C1**−**C8** were recorded in acetonitrile solution. The data are shown in Figure 6 and in Table 3. All potentials are given with respect to ferrocene/ferrocenium redox potential. The first reduction wave for all complexes is reversible, while the reversibility of the second reduction is dependent on the ligand used. As the most cathodic wave was irreversible in the case of **C2** and **C4**, the scan rate was varied from 50 to 1000 mV/s. While this had no effect on **C2**, **C4** showed a reversible signal at high scan rates (above 100 mV/s). On the other hand, the CV of **C2** in DMF at a scan rate of 1000 mV/s displays reversible features (Figure S60 in the Supporting Information). The observed irreversibility might result from a structural or chemical transformation of the system, possibly a decoordination of the ligand upon reduction.

As expected, the measured reduction potential values strongly depend on the ligand structure, spanning over a broad range of ca. 1.0 V (compare **C3** and **C8**). The parent complex **C1** was used as a reference, with E^{red1} = −1.17 V and E^{red2} = −2.04 V. The CV of **C2** (Figure 6) shows that two electron-withdrawing CF_3 groups in the distal position compensate for the effect of one electron-donating $N(CH_3)_2$ group on the central position (**C2**, E^{red1} = −1.24 V and E^{red2} = −1.91 V). Interestingly, the quinoline derivatives **L3** and **L5** (ortho and para isomers) act as electron-deficient ligands, leading to anodically shifted reduction waves (**C3**, E^{red1} = −0.82 V, E^{red2} = −1.61 V; **C5**, E^{red1} = −0.89 V, E^{red2} = −1.68 V). In the case of complex **C4**, the measured redox potential values are found in the range of those of **C1** (**C4**, E^{red1} = −1.32 V, E^{red2} = −2.13 V).

As far as the ligands with dimethylamino groups were concerned, two main conclusions could be drawn. First, as revealed by the similar redox potential values of **C6** and **C7** (**C6**, E^{red1} = −1.54 V; E^{red2} = −2.26 V; **C7**, E^{red1} = −1.52 V; E^{red2} = −2.30 V), the effect of a single substituent on the central pyridyl moiety (**C6**) is equivalent to that of one on each of the distal positions (**C7**). This is consistent with the $Co-N_{cent}$ bond length being ca. 0.2 Å shorter than the $Co-N_{dist}$ lengths, suggesting a stronger interaction of the cobalt with the central pyridyl ring. Second, introducing a dimethylamino group on each of the three rings generates the most electron-rich ligand, **L8**, resulting in very negative potential values for **C8** (E^{red1} = −1.92 V and E^{red2} = −2.49 V). On the basis of these considerations, the electron-donating power of the ligands could be classified as follows: **L8** > **L7** ≈ **L6** > **L4** > **L1** > **L2** > **L5** > **L3**. Interestingly, the very cathodic potential of −2.30 V with full reversibility observed in the case of complex **C7**, combined with its very high solubility in acetonitrile, makes it a promising compound for redox flow battery applications.

Initial attempts to measure the oxidation potential of **C1** were performed under the conditions used for the reduction (glassy-carbon electrode, 0.1 M $TBAClO_4$ electrolyte in acetonitrile, Figure S62 in the Supporting Information). However, the strong increase of current observed at ∼−0.1 V indicated formation of a solid deposit on the electrode. Interestingly, a fully reversible wave was observed when DMF was used as a solvent (Figure S63 in the Supporting Information). This could be overcome in acetonitrile by changing the electrolyte. As shown in Figure S64 in the Supporting Information, lithium bis(trifluoromethane sulfonimidate) (LiTFSI) proved to be the best electrolyte and was further used to study **C2**−**C8** (Figure S64). The choice of electrode material was critical, and thus, we utilized both glassy-carbon and gold electrodes (Figure S65 in the Supporting Information). Specifically in the case of **C2**, no oxidation wave could be detected on a glassy-carbon electrode, while a fully reversible oxidation was observed on a gold electrode. **C1**−**C4** display a fully reversible oxidation with a peak-to-peak separation below 100 mV (Figure S65). **C5**−**C8** have less resolved redox waves, with large peak-to-peak separations and/or irreversibility. Such an electrochemical behavior has been previously observed and is likely due to a slow electron self-exchange rate between the Co^{II} and Co^{III} centers at the electrode surface, in comparison to the electron transfer rate between the electrode and the cobalt ions.[18] The Co(III/II) redox potentials are given in Table 3, and a comparison with other previously reported cobalt bis-terpyridyl systems is given in Figure S66 and Table S4 in the Supporting Information.[18,19] It is shown that this class of systems can span a broad range of potentials, more than 1 V. As expected, in the **C6**−**C8** series the Co(III/II) redox potential is shifting to more cathodic values when more amino substituents are added on the tpy ligand. Interestingly, the potential of **C6** (+0.53 V) was much more positive than that of **R1** (−0.39 V), a previously reported cobalt bis-terpyridyl complex with a *N*-pyrrolidine at the 4-central position (Figure S66 and Table S4). This is likely explained by the strong effect of the methyl groups in **C6**. It appears that the factors governing Co(III/II) redox potentials are rather complex and not straightforward, as strong variations can result from rather minor structural and electronic differences.

The Co(III/II) redox potentials cover a broad range of potentials, varying from −0.21 V to +0.84 V vs Fc^+/Fc. In the context of dye sensitized solar cell applications,[2] the very high oxidation potentials observed with complexes **C5**−**C7** (+0.84, + 0.53, and +0.25 V vs Fc^+/Fc, respectively) could be utilized with various organic photosensitizers.

Quantum Chemical Calculations. Density functional theory (DFT) calculations were performed to investigate the electronic structure of complexes **C1**−**C8** and to better

DOI: 10.1021/acs.inorgchem.7b00595
Inorg. Chem. XXXX, XXX, XXX−XXX

understand the effect of the substituents on the structure and physicochemical properties of the complexes. The electronic and structural properties of $[Co(tpy)_2]^{2+}$, referred to as **C1** in this work, have previously been studied by Wieghardt et al.[20] and Hauser et al.[21]

All systems contained Co(II) ions in a d^7 electronic configuration, thus potentially allowing the existence of two different spin states: a ^2E low-spin doublet and a ^4T high-spin quartet state. Our calculations show that, for all complexes, the quartet states are energetically more favorable (within 6 kcal mol^{-1} for **C1**−**C5** and as high as 9.4, 9.5, and 10.7 kcal mol^{-1} for the three dimethylamino-containing systems **C6**−**C8**, respectively) (Table S5 in the Supporting Information). The optimized geometries are in very good agreement with the experimental X-ray data (Tables 1 and 2), with the Co−N bond lengths within 0.04 Å of the corresponding values in the crystal structure and the angles within 2°. For both doublet and quartet spin states the $Co-N_{cent}$ bond lengths are systematically shorter by ∼0.2 Å in comparison to the $Co-N_{dist}$ lengths, which is in line with our experimental findings. Moreover, the $Co-N_{cent}$ bond lengths vary in the narrow range of 1.90−1.93 Å for the low-spin states, while for the high-spin states these distances are systematically longer by 0.15−0.19 Å, varying in the range of 2.06−2.10 Å. The $Co-N_{dist}$ bond lengths vary slightly in the range of 2.09−2.20 and 2.17−2.28 Å for the low- and high-spin states, respectively. Hence, the $Co-N_{cent}$ bond length can be used as a probe for the spin state of the complex, which is in line with having six-coordinate high- and low-spin Co^{II} ($t_{2g}^6e_g^1$ and $t_{2g}^5e_g^2$) in an octahedral ligand field. In the low-spin complexes, the Jahn−Teller distortion will cause significant tetragonal compression, manifested in elongation of the equatorial metal−ligand ($Co-N_{dist}$) bonds, which coupled with the rigid structure of the tpy ligands will cause the shortening of the $Co-N_{cent}$ bond lengths. Our findings are in agreement with previous results on cobalt polypyridyl based complexes ($[Co(tpy)_2]^{2+}$, $[Co(^tbpy)_3]^{2+}$, and $[Co(phen)_3]^{2+}$,[20] as well as $[Co(tpy)_2]^{2+}$ and $[Co(bpy)_3]^{2+}$ [21]). A closer inspection of Table 2 thus reveals that best agreement with our crystal structures is obtained when complexes **C1**−**C3** and **C5**−**C8** are in their high-spin quartet state, while only **C4** is best described as a low-spin doublet. One should note that, as demonstrated for **C1**, the spin state is strongly influenced by the environment of the complex, depending on parameters such as the nature of the counterion, the nature and number of solvent molecules in crystalline media or solution, and the temperature.[22] Table 1 shows that the computed acute α and obtuse β $N_{dist}-Co-N_{dist}$ angles are also in excellent agreement with the experimental values, except for complex **C5**. The two **L5** ligands in complex **C5** deviate significantly from orthogonality, due to favorable $\pi-\pi$ stacking between the *p*-quinoline moieties (see Figure S75 in the Supporting Information). Test calculations with different DFT functionals, such as B3LYP-D3, B97D, and M06, predicted virtually the same geometry. A closer inspection of the **C5** crystal structure revealed that such dispersive interactions are prevented by the existence of four aromatic rings: two toluene solvent molecules and two central pyridyl units from the neighboring **C5** complexes in the unit cell. We have thus performed an optimization of **C5** with four toluene molecules between the quinoline ligands, and indeed the perpendicular arrangement of the **L5** ligands is maintained, in good agreement with the experimental structure (see Table 1).

The DFT-computed descriptors also indicate that the ligands in all complexes deviate significantly from planarity, except for both spin states of **C2** and **C4**. In **C5** the *p*-quinoline units are 1.0−1.2 Å out of the plane (experimental $d_{2,3}$ values are ±0.4 Å), which is corrected to the largest deviation of ∼0.7 Å when four solvent molecules are explicitly included in the geometry optimization of the complex. Even greater deviation from planarity of the ligands is calculated for the *o*-quinoline-based complex **C3** (d_1 = 1.30 Å vs the corresponding experimental value of 1.14 Å), owing to the large steric repulsion of hydrogens from the central and distal pyridyl rings within each ligand **L3**. Introducing two electron-withdrawing CF_3 groups on the distal pyridyl units along with a single electron-donating $N(CH_3)_2$ group on the central ring in **C2** has virtually no effect on the geometry, and the structure remains essentially identical with that of **C1**. For the terpyridines containing dimethylamino groups, **C6**−**C8**, our calculations consistently find distortion of planarity for their doublet spin states by ∼0.6 Å in terms of d_2 and d_3 descriptors, while d_1 = 0. The high-spin-state structures are more planar (displacements of ∼0.4 Å maximum), with the largest deviations found for the d_3 values in the range of 0.6−0.8 Å.

The spin density plots of complexes **C1**−**C8** (Figures S67−S74 in the Supporting Information) reveal the dominant contribution of Co(II), with ρ = 0.97−0.99 in the low-spin doublet state and ρ = 2.73−2.87 in the high-spin quartet state and very little density on the pyridyl N atoms. Figures S67−S74 show the frontier molecular orbitals of complexes **C1**−**C8**. The low-spin doublet states are characterized by a HOMO that is a pure Co 3d orbital, except in **C2** and **C6**, where the $N(CH_3)_2$ groups at the central rings introduce an axial symmetry and the HOMO is composed of Co 3d and C and N 2p orbitals in the same plane. The singly occupied MO (SOMO) is the σ^* antibonding $Co-N_{dist}$ orbital composed of Co $3d_{x^2-y^2}$ and N_{dist} 2p, while the LUMO orbital is the σ^* antibonding $Co-N_{cent}$ orbital composed of Co $3d_{z^2}$ and N_{cent} 2p. As far as the high-spin quartets are concerned, the HOMO orbital is either a ligand-based orbital (**C1**, **C3**, **C5**, **C7**, and **C8**) or an antibonding $Co-N_{dist}$ orbital composed of Co $3d_{x^2-y^2}$ and N 2p as in **C2**, **C4**, and **C6**. The three unpaired electrons reside on two ligand-based orbitals and the $Co-N_{cent}$ σ^* antibonding orbitals of Co $3d_{z^2}$, while the LUMO is always a ligand-based orbital. Thus, the main difference in the spin states in all complexes **C1**−**C8** is the population of the Co $3d_{z^2}$ orbital in the quartet states, decreasing the back-bonding of Co to the central pyridyl ring, thus providing an explanation of the change in the $Co-N_{cent}$ distance, which is elongated by ∼0.2 Å when passing from a low-spin to a high-spin state.

Finally, our calculations show that the first electron reduction of complexes **C1**−**C8** is always metal-based and corresponds to the reduction of Co^{II} to Co^{I}, with an electron occupying the antibonding σ^* $Co-N_{cent}$ orbital (having mainly $3d_{z^2}$ character). The second reduction, on the other hand, corresponds to a ligand-based event (see Figure 6). While in **C1** the electron is delocalized over the entire ligands, in **C2** it is localized on the distal rings due to the electron-withdrawing CF_3 groups and in the quinoline-based **C3**−**C5** complexes it is localized primarily on the central ring, involving parts of the distal quinoline rings, but not the terminal phenyl rings (**C5**). Similarly, in the dimethylamino-substituted complexes **C7** and **C8** the electron resides on the central ring, whereas in **C6** it is delocalized on the entire **L6** ligand.

DOI: 10.1021/acs.inorgchem.7b00595
Inorg. Chem. XXXX, XXX, XXX−XXX

CONCLUSIONS

We have synthesized a series of new terpyridine ligands bearing a variety of substituting moieties using Stille cross-coupling reactions. The corresponding bis-substituted Co(II) complexes were isolated and fully characterized. The crystal structures revealed distortions in some of these systems, especially when the terpyridine ligands were functionalized with different substituents. The DFT calculations provided insight into understanding the differences of Co−N bond lengths observed in the crystal structures, assigning them to differences in terms of spin states. In particular, the Co−N_{cent} bond length can be used as a probe for differentiating the low-spin doublet from the high-spin quartet state. In this work, we have shown that the redox potential of the Co(III)/Co(II), Co(II)/Co(I), and Co(I)/Co(I) $(tpy)^{\bullet-}$ couples can be easily modulated over 1 V by tuning the substituents on the tpy ligands, allowing a broad range of applications. Study of the catalytic properties of this class of complexes is currently ongoing.

EXPERIMENTAL SECTION

General Considerations. NMR spectra were recorded on a Bruker AVANCE III 300 spectrometer (Bruker BioSpin GmbH, Rheinstetten, Germany). HR-ESI-MS spectra were recorded in positive mode on a Waters LCT Premier XE mass spectrometer equipped with an electrospray ionization source. The ionization was carried out in positive mode in the m/z 80−1500 range. LR-ESI-MS spectra of the molecular complexes were recorded in positive mode on a PE Sciex API 3000 mass spectrometer equipped with an electrospray ionization source. UV−vis spectra were recorded on a Cary100 UV−vis spectrophotometer (Agilent Technologies, Santa Clara, CA, USA). Suitable crystals of the complexes were mounted in Paratone oil and transferred into a cold nitrogen gas stream. Intensity data were collected with Bruker Kappa-APEX2 systems using microsource Cu Kα or fine-focus sealed-tube Mo Kα radiation or using an Oxford Diffraction XCallibur S κ geometry diffractometer (Mo Kα radiation, graphite monochromator, λ = 0.71073 Å). Data collection was carried out with the Bruker APEX2 suite of programs (APEX2 diffractometer) and by CrysAlisPro Oxford Diffraction software (XCallibur diffractometer). Unit-cell parameter determination, integration, and data reduction were performed with SAINT (APEX II). Alternatively, unique intensities detected on all frames using the Oxford Diffraction Red program were used to refine the values of the cell parameters (XCallibur). SADABS[23] (APEX II) and the ABSPACK Oxford Diffraction programs were used for scaling and multiscan absorption corrections. The structures were solved with WinGX and Olex2 1.2 using the SHELXT-2014[24] package and refined by full-matrix least-squares methods with SHELXL-2014. All non-hydrogen atoms were refined anisotropically. Hydrogen atoms were placed at calculated positions and refined with a riding model. Electrochemical measurements were performed using a Bio-Logic SP300 potentiostat model (Bio-Logic, Claix, France). CVs were recorded in a glovebox to prevent oxygen. An electrochemical cell with a glassy-carbon electrode as a working electrode (i.d. 1.0 mm), a platinum wire as a counter electrode (i.d. 1 mm), and a silver wire in silver nitrate isolated from the solution using a Vycor frit (10 mM in 0.1 M $TBAClO_4$ solution in acetonitrile) as a reference electrode in a 3.0 mL solution was used to measure the CVs. A gold working electrode (i.d. 3.0 mm) was also used when stated. FT-IR spectra were recorded on a IR Prestige-21 spectrometer with Universal ATR Sampling Accessory (Shimadzu, Kyoto, Japan). Purifications with flash liquid chromatography were carried out using a Reveleris X2 system (Grace, Columbia, USA) equipped with disposable silica columns. For synthesis, the solutions were degassed (when mentioned) by bubbling argon in the solution for at least 20 min. Dry solvents (when mentioned) were obtained using a MBraun Solvent Purification System.

Computational Methods. Molecular geometries were optimized at the M06-L[25]/6-311+G(d,p)[26] level of density functional theory using the Gaussian 09 software package.[27] A quasi-relativistic Stuttgart/Dresden effective core potential was used on Co.[28] The integral evaluation made use of the grid defined as "ultrafine" in G09. Frequency calculations on optimized geometries ensured that structures were minima (zero imaginary frequency) on the potential energy surface.

Synthesis of L2. In a Schlenk flask, a toluene solution (7.0 mL) of **S3** (181 mg, 0.485 mmol) and **S9** (0.635 g, 1.45 mmol) was degassed under argon for 15 min. The catalyst $[Pd(PPh_3)_4]$ (47.0 mg, 0.042 mmol) was added, and the solution was degassed again under argon for 15 min. The solution was heated at 110 °C for 96 h. The solvent was removed under vacuum, and the residue was purified by column chromatography (cyclohexane/ethyl acetate gradient) to yield **L2** as a white powder (103 mg, 0.25 mmol, 52%). IR (ATR): ν_{max} (cm^{-1}) 2926 (w), 2854 (w), 2816 (w), 1589 (w), 1541 (w), 1506 (w), 1471 (w), 1431 (w), 1413 (w), 1379 (w), 1328 (w), 1276 (w), 1253 (w), 1228 (w), 1165 (w), 1124 (m), 1070 (w), 1004 (w), 991 (w), 975 (w), 920 (w), 894 (w), 840 (m), 788 (w), 700 (w), 663 (m), 607 (w). ^{1}H NMR (300 MHz, $CDCl_3$): δ 3.34 (s, 3H), 7.59 (d, J = 5.0 Hz, 2H), 7.91 (s, 2H), 8.8−9.0 (m, 2H). ^{13}C NMR (75 MHz, $CDCl_3$): δ 40.28, 104.93, 117.67, 119.72, 124.68, 149.86 (2C), 156.00−157.5 (3C). HR-MS (ESI+): m/z calcd for $C_{19}H_{15}F_6N_4^+$ 413.1195, found 413.1201 ($[M + H]^+$).

Synthesis of L3. In a Schlenk flask, a toluene solution (18 mL) of **S5** (0.53 g, 1.3 mmol) and **S10** (1-chloroisoquinoline) (1.0 g, 3.9 mmol, Fluorochem) was degassed under argon for 15 min. The catalyst $[Pd(PPh_3)_4]$ (0.153 g, 0.13 mmol) was added, and the solution was degassed again under argon for 15 min. The solution was heated at 110 °C for 96 h. The solvent was removed under vacuum, and the residue was purified by column chromatography (cyclohexane/ethyl acetate gradient). The isolated product was recrystallized in acetonitrile and dried under vacuum to yield **L3** as a white powder (191 mg, 0.57 mmol, 44%). IR (ATR): ν_{max} (cm^{-1}) 3043 (w), 3007 (w), 2924 (w), 2852 (w), 1568 (w), 1435 (w), 1373 (w), 1346 (w), 1319 (w), 1249 (w), 1238 (w), 1215 (w), 1126 (w), 1089 (w), 1022 (w), 952 (w), 916 (w), 869 (w), 835 (w), 819 (w), 798 (w), 789 (w), 734 (w), 704 (w), 669 (w). ^{1}H NMR (300 MHz, $CDCl_3$): δ 7.51 (t, J = 7.5 Hz, 2H), 7.68 (t, J = 7.5 Hz, 2H), 7.76 (d, J = 5.5 Hz, 2H), 7.88 (d, J = 7.5 Hz, 2H), 8.16 (s, 3H), 8.68 (d, J = 5.5 Hz, 2H), 8.75 (d, J = 7.5 Hz, 2H). ^{13}C NMR (75 MHz, $CDCl_3$): δ 121.40, 124.81, 126.84, 126.91, 127.62, 128.13, 130.13, 137.19, 137.89, 141.81, 157.32, 157.48. HR-MS (ESI+): m/z calcd for $C_{23}H_{16}N_3^+$ 334.1339, found 334.1344 ($[M + H]^+$).

Synthesis of L4. In a Schlenk flask, a toluene solution (18 mL) of **S5** (0.53 g, 1.3 mmol) and **S11** (3-chloroisoquinoline) (1.0 g, 3.9 mmol, Fluorochem) was degassed under argon for 15 min. The catalyst $[Pd(PPh_3)_4]$ (0.153 g, 0.13 mmol) was added, and the solution was degassed again under argon for 15 min. The solution was heated at 110 °C for 96 h. The solvent was removed in vacuo, and the residue was purified by column chromatography (cyclohexane/ethyl acetate gradient). The isolated product was recrystallized in acetonitrile and dried under vacuum to yield **L4** as a white powder (170 mg, 0.51 mmol, 39%). IR (ATR): ν_{max} (cm^{-1}) 3057 (w), 3024 (w), 2980 (w), 2964 (w), 2926 (w), 2854 (w), 1625 (w), 1581 (w), 1562 (w), 1492 (w), 1463 (w), 1438 (w), 1427 (w), 1386 (w), 1342 (w), 1267 (w), 1255 (w), 1236 (w), 1192 (w), 1136 (w), 945 (w), 900 (w), 885 (w), 850 (w), 817 (m), 734 (m), 675 (w). ^{1}H NMR (300 MHz, $CDCl_3$): δ 7.64 (t, J = 7.5 Hz, 2H), 7.76 (t, J = 7.5 Hz, 2H), 8.06 (m, 5H), 8.56 (d, J = 7.5 Hz, 2H), 9.06 (s, 2H), 9.37 (s, 2H). ^{13}C NMR (75 MHz, $CDCl_3$): δ 117.78, 120.93, 127.57, 127.65, 127.75, 128.81, 130.55, 136.69, 137.98, 150.19, 152.08, 155.95. HR-MS (ESI+): m/z calcd for $C_{23}H_{16}N_3^+$ 334.1339, found 334.1344 ($[M + H]^+$).

Synthesis of L5. In a Schlenk flask, a toluene solution (12 mL) of **S5** (0.36 g, 0.89 mmol) and **S7** (2-iodoquinoline) (0.60 g, 2.67 mmol, Fluorochem) was degassed under argon for 15 min. The catalyst $[Pd(PPh_3)_4]$ (0.104 g, 0.09 mmol) was added, and the solution was degassed again under argon for 15 min. The solution was heated at 110 °C for 96 h. The solvent was removed under vacuum, and the residue was purified by column chromatography (cyclohexane/ethyl acetate gradient) to yield **L5** as a yellowish powder (282 mg, 0.84

DOI: 10.1021/acs.inorgchem.7b00595
Inorg. Chem. XXXX, XXX, XXX−XXX

mmol, 94%). IR (ATR): ν_{max} (cm^{-1}) 3051 (w), 2995 (w), 2895 (w), 2798 (w), 2763 (w), 2742 (w), 2655 (w), 1616 (w), 1595 (m), 1556 (m), 1502 (m), 1433 (m), 1423 (m), 1321 (w), 1305 (w), 1247 (w), 1236 (w), 1122 (m), 1084 (m), 1060 (w), 1014 (w), 993 (w), 956 (w), 941 (w), 831 (m), 815 (m), 785 (m), 733 (m), 771 (w). ^{1}H NMR (300 MHz, $CDCl_3$): δ 7.85 (t, J = 7.5 Hz, 2H), 7.77 (t, J = 7.5 Hz, 2H), 7.89 (d, J = 8.5 Hz, 2H), 8.08 (t, J = 7.5 Hz, 1H), 7.22 (d, J = 8.5 Hz, 2H), 8.35 (d, J = 8.5 Hz, 2H), 7.78 (d, J = 7.5 Hz, 2H), 8.85 (d, J = 8.5 Hz, 2H). HR-MS (ESI+): m/z calcd for $C_{23}H_{16}N_3^+$ 334.1339, found 334.1344 ($[M + H]^+$).

Synthesis of L6. In a Schlenk flask, a toluene solution (2.5 mL) of **S3** (65.0 mg, 0.175 mmol) and **S12** (2-methyl-6-(tributylstannyl)-pyridine) (0.20 g, 0.523 mmol, Sigma-Aldrich) was degassed under argon for 15 min. The catalyst $[Pd(PPh_3)_4]$ (17.0 mg, 0.015 mmol) was added and the solution was degassed again under argon for 15 min. The solution was heated at 110 °C for 96 h. The solvent was removed in vacuo, and the residue was purified by column chromatography (cyclohexane/ethyl acetate gradient) to yield **L6** as a white powder (20 mg, 0.065 mmol, 37%). IR (ATR): ν_{max} (cm^{-1}) 2985 (w), 2922 (w), 2885 (w), 2802 (w), 1608 (w), 1570 (w), 1541 (w), 1506 (w), 1423 (w), 1411 (w), 1226 (w), 1141 (w), 1082 (w), 983 (w), 852 (w), 800 (w), 744 (w), 698 (w), 661 (w), 638 (w). ^{1}H NMR (300 MHz, $CDCl_3$): δ 7.14 (d, J = 7.5 Hz, 2H), 7.71 (t, J = 7.5 Hz, 2H), 7.76 (s, 2H), 8.39 (d, J = 7.5 Hz, 2H). ^{13}C NMR (75 MHz, $CDCl_3$): δ 24.70, 39.64, 103.72, 118.49, 122.95, 136.68, 155.78, 156.42, 157.52 (2C). HR-MS (ESI+): m/z calcd for $C_{19}H_{21}N_4^+$ 305.1761, found 305.1766 ($[M + H]^+$).

General Procedure for the Synthesis of Molecular Complexes (except C5). To a solution of anhydrous $CoCl_2$ (1.0 equiv, Sigma-Aldrich) in degassed methanol (1.0 mL/15 μmol $CoCl_2$) was added a powder of the terpyridyl ligand (2.0 equiv). The solution was refluxed for 3 h under argon and cooled to room temperature. The complex was precipitated after addition of a concentrated aqueous solution of ammonium hexafluorophosphate (8.0 equiv, Sigma-Aldrich), and the product was collected by filtration. The product was thoroughly washed with 20 mL portions of water (Milli-Q), toluene, and Et_2O. The obtained powder was dissolved in a minimum amount of acetone, and toluene was added dropwise until the complex precipitated. The precipitate was collected and dried under vacuum to provide **C1**−**C8**.

Synthesis of C5. To a solution of anhydrous $CoCl_2$ (1.0 equiv, Sigma-Aldrich) in degassed methanol (1.0 mL/7.5 μmol $CoCl_2$) was added a powder of the terpyridyl ligand (2.0 equiv). The solution was refluxed for 3 h under argon and cooled to room temperature. A concentrated solution of ammonium hexafluorophosphate (8.0 equiv, Sigma-Aldrich) in methanol was added, and the solvent was removed with a rotary evaporator. The product was thoroughly washed with 20 mL portions of water (Milli-Q), toluene, and Et_2O. The obtained powder was dissolved in a minimum amount of acetone, and toluene was added dropwise until the complex precipitated. The precipitate was collected and dried under vacuum to provide **C5**.

C1: isolated yield 93%. ^{1}H NMR (300 MHz, CD_3CN): δ 98.88, 56.77, 48.24, 33.97, 21.25, 8.39. IR (ATR): ν_{max} (cm^{-1}) 3130 (w), 3095 (w), 2972 (w), 2900 (w), 2885 (w), 1600 (w), 1577 (w), 1473 (w), 1452 (w), 1436 (w), 1323 (w), 1244 (w), 1193 (w), 1051 (w), 1029 (w), 1014 (w), 902 (w), 879 (w), 837 (s), 819 (s), 767 (s), 740 (w), 729 (w), 690 (w). Anal. Calcd for $C_{30}H_{22}CoF_{12}N_6P_2$: C, 44.19; H, 2.72; N, 10.31. Found: C, 44.33; H, 2.66; N, 10.28. LRMS (ESI^+): m/z 670.3 ($[M - PF_6]^+$), 262.6 ($[M - 2PF_6]^{2+}$).

C2: isolated yield 82%. ^{1}H NMR (300 MHz, CD_3CN): 99.66, 83.20, 68.40, 25.24, 23.75; IR (ATR): ν_{max} (cm^{-1}) 2987 (w), 2972 (w), 2891 (w), 1616 (w), 1533 (w), 1506 (w), 1417 (w), 1330 (m), 1288 (w), 1265 (w), 1230 (w), 1178 (w), 1165 (w), 1138 (w), 1089 (w), 1029 (w), 900 (w), 823 (s), 734 (w), 680 (m), 665 (w); Anal. Calcd for $C_{41}H_{34}CoF_{24}N_8OP_2$ (**C2**•CH_3COCH_3): C, 39.98; H, 2.78; N, 9.10. Found: C, 40.31; H, 2.63; N, 8.95. LRMS (ESI^+), m/z: 1028.4 ($[M - PF_6]^+$), 441.9 ($[M - 2PF_6]^{2+}$).

C3: isolated yield 77%; ^{1}H NMR (300 MHz, CD_3CN): δ 105.71, 67.45, 40.06, 15.79, 13.88, 9.61, 6.80, 2.09. IR (ATR): ν_{max} (cm^{-1}) 3082 (w), 2972 (w), 2895 (w), 1705 (w), 1622 (w), 1585 (w), 1573 (w), 1552 (w), 1471 (w), 1456 (w), 1386 (w), 1354 (w), 1311 (w), 1271 (w), 1222 (w), 1186 (w), 1020 (w), 875 (w), 833 (s), 821 (s), 740 (w), 667 (w). Anal. Calcd for $C_{53}H_{38}CoF_{12}N_6P_2$ (**C3**·PhMe): C, 57.46; H, 3.46; N, 7.59. Found: C, 57.36; H, 3.35; N, 7.25. LRMS (ESI^+): m/z 870.6 ($[M - PF_6]^+$), 362.7 ($[M - 2PF_6]^{2+}$).

C4: isolated yield 71%. ^{1}H NMR (300 MHz, CD_3CN): δ 111.46, 55.40, 46.74, 21.27, 10.15, 9.27, 7.96, 7.89, 6.08. IR (ATR): ν_{max} (cm^{-1}) 3093 (w), 2972 (w), 2885 (w), 1625 (w), 1602 (w), 1568 (w), 1505 (w), 1489 (w), 1446 (w), 1390 (w), 1298 (w), 1269 (w), 1174 (w), 968 (w), 831 (s), 810 (s), 758 (w), 736 (w), 678 (w). Anal. Calcd for $C_{53}H_{38}CoF_{12}N_6P_2$ (**C4**·PhMe): C, 57.46; H, 3.46; N, 7.59. Found: 57.24; H, 3.36; N, 7.29. LRMS (ESI^+): m/z 870.7 ($[M - PF_6]^+$), 362.7 ($[M - 2PF_6]^{2+}$).

C5: isolated yield 90%. ^{1}H NMR (300 MHz, CD_3CN): δ 98.64, 72.23, 27.88, 24.14, 14.77, 4.95, 3.75, 2.33. IR (ATR): ν_{max} (cm^{-1}) 3093 (w), 2972 (w), 2893 (w), 1593 (w), 1516 (w), 1485 (w), 1435 (w), 1379 (w), 1342 (w), 1271 (w), 1220 (w), 1195 (w), 1148 (w), 1101 (w), 1083 (w), 1029 (w), 877 (w), 825 (s), 806 (s), 779 (m), 761 (m), 738 (m), 686 (w). Anal. Calcd for $C_{53}H_{38}CoF_{12}N_6P_2$ (**C5**·PhMe): C, 57.46; H, 3.46; N, 7.59. Found: C, 57.18; H, 3.43; N, 7.27. LRMS (ESI^+): m/z 870.7 ($[M - PF_6]^+$), 362.8 ($[M - 2PF_6]^{2+}$).

C6: isolated yield 86%. ^{1}H NMR (300 MHz, CD_3CN): δ 113.79, 77.10, 35.85, 20.17, −0.95, −11.67. IR (ATR): ν_{max} (cm^{-1}) 2972 (w), 2900 (w), 1618 (w), 1604 (w), 1573 (w), 1533 (w), 1456 (w), 1438 (w), 1379 (w), 1307 (w), 1251 (w), 1166 (w), 1114 (w), 1070 (w), 1047 (w), 997 (w), 906 (w), 873 (w), 831 (s), 800 (m), 742 (w), 651 (w). Anal. Calcd for $C_{41}H_{46}CoF_{12}N_8OP_2$ (**C6**·CH_3COCH_3): C, 48.48; H, 4.56; N, 11.03. Found: C, 48.32; H, 4.50; N, 10.93. LRMS (ESI^+): m/z 812.3 ($[M - PF_6]^+$), 333.7 ($[M - 2PF_6]^{2+}$).

C7: isolated yield 88%. ^{1}H NMR (300 MHz, CD_3CN): δ 61.01, 58.65, 45.21, 8.87, 7.07, −7.92. IR (ATR): ν_{max} (cm^{-1}) 2933 (w), 2895 (w), 2818 (w), 1610 (w), 1573 (w), 1521 (m), 1506 (w), 1489 (w), 1436 (w), 1417 (w), 1384 (w), 1369 (w), 1311 (w), 1271 (w), 1232 (w), 1186 (w), 1166 (w), 1143 (w), 1126 (w), 1105 (w), 1066 (w), 1047 (w), 985 (w), 829 (s), 813 (s), 738 (w), 694 (w). Anal. Calcd for $C_{42}H_{50}CoF_{12}N_{10}P_2$: C, 48.33; H, 4.83; N, 13.42. Found: C, 47.89; H, 4.89; N, 13.30. LRMS (ESI^+): m/z 898.8 ($[M - PF_6]^+$), 376.3 ($[M - 2PF_6]^{2+}$).

C8: isolated yield 74%. ^{1}H NMR (300 MHz, CD_3CN): δ 87.28, 67.31, 29.45, 19.16, 1.76, −9.82. IR (ATR): ν_{max} (cm^{-1}) 2972 (w), 2931 (w), 2893 (w), 2818 (w), 1608 (m), 1537 (w), 1506 (m), 1427 (w), 1367 (w), 1232 (w), 1178 (w), 1155 (w), 1045 (w), 989 (w), 821 (s), 810 (s), 707 (w). Anal. Calcd for $C_{46}H_{60}CoF_{12}N_{12}P_2$: C, 48.90; H, 5.35; N, 14.88. Found: C, 46.76; H, 5.15; N, 14.29. LRMS (ESI^+): m/z 984.9 ($[M - PF_6]^+$), 420.1 ($[M - 2PF_6]^{2+}$).

■ ASSOCIATED CONTENT

Supporting Information

The Supporting Information is available free of charge on the ACS Publications website at DOI: 10.1021/acs.inorgchem.7b00595.

Synthetic procedures of **L2**−**L6** and **C1**−**C8**, NMR spectra of **L2**−**L6** and **C1**−**C8**, MS spectra of **L2**−**L6** and **C1**−**C8**, UV−vis spectra of **L1**−**L8** and **C1**−**C8**, buried volumes of **C1**−**C8**, cyclic voltammetry experiments of **C1**−**C8** for Co(III/II) couple, and computational details for **C1**−**C8** (PDF)

Crystallographic data for **C1** and **C3**−**C8** (ZIP)

■ AUTHOR INFORMATION

Corresponding Author

*E-mail for M.F.: marc.fontecave@college-de-france.fr.

ORCID

Marc Fontecave: 0000-0002-8016-4747

Notes

The authors declare no competing financial interest.

DOI: 10.1021/acs.inorgchem.7b00595
Inorg. Chem. XXXX, XXX, XXX−XXX

■ ACKNOWLEDGMENTS

We acknowledge support from Foundation de l'Orangerie for individual Philanthropy and its donors. This work was supported by the French National Research Agency (ANR, Carbiored ANR-12-BS07-0024-03). This work has benefited from the facilities and expertise of the Small Molecule Mass Spectrometry platform of ICSN (Centre de Recherche de Gif - www.icsn.cnrs-gif.fr). P.H. and H.-U.R. acknowledge the Deutsche Forschungsgemeinschaft for support. The calculations were performed using the HPC resources of GENCI (TGCC) through Grant 2017-810082.

■ REFERENCES

(1) (a) Shepard, S. G.; Fatur, S. M.; Rappe, A. K.; Damrauer, N. H. Highly Strained Iron(II) Polypyridines: Exploiting the Quintet Manifold To Extend the Lifetime of MLCT Excited States. *J. Am. Chem. Soc.* **2016**, *138*, 2949−2952. (b) Brown, D. G.; Sanguantrakun, N.; Schulze, B.; Schubert, U. S.; Berlinguette, C. P. Bis(tridentate) Ruthenium−Terpyridine Complexes Featuring Microsecond Excited-State Lifetimes. *J. Am. Chem. Soc.* **2012**, *134*, 12354−12357. (c) Lin, H. W.; Wang, Y. S.; Huang, Z. Y.; Lin, Y. M.; Chen, C. W.; Yang, S. H.; Wu, K. L.; Chi, Y.; Liu, S. H.; Chou, P. T. Origins of device performance in dicarboxyterpyridine Ru(II) dye-sensitized solar cells. *Phys. Chem. Chem. Phys.* **2012**, *14*, 14190−14195.

(2) (a) Yum, J. H.; Baranoff, E.; Kessler, F.; Moehl, T.; Ahmad, S.; Bessho, T.; Marchioro, A.; Ghadiri, E.; Moser, J. E.; Yi, C. Y.; Nazeeruddin, M. K.; Gratzel, M. A cobalt complex redox shuttle for dye-sensitized solar cells with high open-circuit potentials. *Nat. Commun.* **2012**, *3*, 631. (b) Sapp, S. A.; Elliott, C. M.; Contado, C.; Caramori, S.; Bignozzi, C. A. Substituted polypyridine complexes of cobalt(II/III) as efficient electron-transfer mediators in dye-sensitized solar cells. *J. Am. Chem. Soc.* **2002**, *124*, 11215−11222. (c) Hamann, T. W. The end of iodide? Cobalt complex redox shuttles in DSSCs. *Dalton. Trans.* **2012**, *41*, 3111−3115. (d) Stergiopoulos, T.; Falaras, P. Minimizing Energy Losses in Dye-Sensitized Solar Cells Using Coordination Compounds as Alternative Redox Mediators Coupled with Appropriate Organic Dyes. *Adv. Energy Mater.* **2012**, *2*, 616−627.

(3) Sevov, C. S.; Fisher, S. L.; Thompson, L. T.; Sanford, M. S. Mechanism-Based Development of a Low-Potential, Soluble, and Cyclable Multielectron Anolyte for Nonaqueous Redox Flow Batteries. *J. Am. Chem. Soc.* **2016**, *138*, 15378−15384.

(4) Fermi, A.; Bergamini, G.; Roy, M.; Gingras, M.; Ceroni, P. Turn-on Phosphorescence by Metal Coordination to a Multivalent Terpyridine Ligand: A New Paradigm for Luminescent Sensors. *J. Am. Chem. Soc.* **2014**, *136*, 6395−6400.

(5) Li, C.; Fan, W.; Straus, D. A.; Lei, B.; Asano, S.; Zhang, D. H.; Han, J.; Meyyappan, M.; Zhou, C. W. Charge Storage Behavior of Nanowire Transistors Functionalized with Bis(terpyridine)-Fe(II) Molecules: Dependence on Molecular Structure. *J. Am. Chem. Soc.* **2004**, *126*, 7750−7751.

(6) (a) Zheng, Z. K.; Opilik, L.; Schiffmann, F.; Liu, W.; Bergamini, G.; Ceroni, P.; Lee, L. T.; Schutz, A.; Sakamoto, J.; Zenobi, R.; VandeVondele, J.; Schluter, A. D. Synthesis of Two-Dimensional Analogues of Copolymers by Site-to-Site Transmetalation of Organometallic Monolayer Sheets. *J. Am. Chem. Soc.* **2014**, *136*, 6103−6110. (b) Groger, G.; Meyer-Zaika, W.; Bottcher, C.; Grohn, F.; Ruthard, C.; Schmuck, C. Switchable Supramolecular Polymers from the Self-Assembly of a Small Monomer with Two Orthogonal Binding Interactions. *J. Am. Chem. Soc.* **2011**, *133*, 8961−8971. (c) Schubert, U. S.; Eschbaumer, C. Macromolecules containing bipyridine and terpyridine metal complexes: Towards metallosupramolecular polymers. *Angew. Chem., Int. Ed.* **2002**, *41*, 2892−2926.

(7) Tan, J. Y.; Li, R.; Li, D. D.; Zhang, Q.; Li, S. L.; Zhou, H. P.; Yang, J. X.; Wu, J. Y.; Tian, Y. P. Thiophene-based terpyridine and its zinc halide complexes: third-order nonlinear optical properties in the near-infrared region. *Dalton. Trans.* **2015**, *44*, 1473−1482.

(8) (a) Elgrishi, N.; Chambers, M. B.; Fontecave, M. Turning it off! Disfavouring hydrogen evolution to enhance selectivity for CO production during homogeneous CO_2 reduction by cobalt-terpyridine complexes. *Chem. Sci.* **2015**, *6*, 2522−2531. (b) Elgrishi, N.; Griveau, S.; Chambers, M. B.; Bedioui, F.; Fontecave, M. Versatile functionalization of carbon electrodes with a polypyridine ligand: metallation and electrocatalytic H^+ and CO_2 reduction. *Chem. Commun.* **2015**, *51*, 2995−2998.

(9) Elgrishi, N.; Chambers, M. B.; Artero, V.; Fontecave, M. Terpyridine complexes of first row transition metals and electrochemical reduction of CO_2 to CO. *Phys. Chem. Chem. Phys.* **2014**, *16*, 13635−13644.

(10) Colombe, J. R.; Bernhardt, S.; Stathakis, C.; Buchwald, S. L.; Knochel, P. Synthesis of Solid 2-Pyridylzinc Reagents and Their Application in Negishi Reactions. *Org. Lett.* **2013**, *15*, 5754−5757.

(11) Morgan, G. T.; Burstall, F. H. 3. Dehydrogenation of Pyridine of Anhydrous Ferric Chloride. *J. Chem. Soc.* **1932**, 20−30.

(12) (a) Rosevear, P. E.; Sasse, W. H. F. Synthesis of some 4,4′,4″-trialkyl-2,2′6′,2″-terpyridyls. *J. Heterocycl. Chem.* **1971**, *8*, 483−485. (b) Ben Hadda, T.; Le Bozec, H. Synthesis and characterization of ruthenium(II) complexes containing the new tridentate ligand 4,4′,4″-tri-tert-butyl-terpyridine. *Inorg. Chim. Acta* **1993**, *204*, 103−107. (c) Robo, M. T.; Prinsell, M. R.; Weix, D. J. 4,4 ′,4 ″-Trimethy1−2,2 ′:6 ′,2 ″-terpyridine by Oxidative Coupling of 4-Picoline. *J. Org. Chem.* **2014**, *79*, 10624−10628.

(13) Sasaki, I.; Daran, J. C.; Balavoine, G. G. A. An Effective Route to Polysubstituted Symmetric Terpyridines. *Synthesis* **1999**, *1999*, 815−820.

(14) (a) Louerat, F.; Gros, P. C. Functional polypyridine ligands from copper-mediated room temperature coupling of 4-chloro-2-trimethylsilylpyridine. *Tetrahedron Lett.* **2010**, *51*, 3558−3560. (b) Harzmann, G. D.; Neuburger, M.; Mayor, M. 4,4-Disubstituted Terpyridines and Their Homoleptic Fe^{II} Complexes. *Eur. J. Inorg. Chem.* **2013**, *2013*, 3334−3347. (c) Cardenas, D. J.; Sauvage, J. P. Improved Synthesis of 2,6-Oligopyridines by Stille Cross-coupling Reaction. *Synlett* **1996**, *1996*, 916−918. (d) Schubert, U. S.; Eschbaumer, C. New Synthetic Strategy toward Pyridine-Based Ligands for Supramolecular Chemistry Utilizing 2,6-Bis(trimethyltin)-pyridine as the Central Building Block. *Org. Lett.* **1999**, *1*, 1027−1029.

(15) (a) Hommes, P.; Fischer, C.; Lindner, C.; Zipse, H.; Reissig, H. U. Unprecedented Strong Lewis Bases−Synthesis and Methyl Cation Affinities of Dimethylamino-Substituted Terpyridines. *Angew. Chem., Int. Ed.* **2014**, *53*, 7647−7651. (b) Hommes, P.; Reissig, H.-U. Synthesis and Photophysical Properties of Substituted 2,2′:6′,2″-Terpyridine Derivatives and Analogous Compounds with a Central Thiophene Ring. *Asian J. Org. Chem.* **2016**, *5*, 1033−1040. (c) De Rache, A.; Gueddouda, N. M.; Bourdoncle, A.; Hommes, P.; Reissig, H. U.; Mergny, J. L. A Flexible Terpyridine Derivative Interacts Specifically with G-Quadruplexes. *Chem. - Eur. J.* **2016**, *22*, 12651−12654.

(16) Arana, C.; Yan, S.; Keshavarzk, M.; Potts, K. T.; Abruna, H. D. Electrocatalytic Reduction of Carbon Dioxide with Iron, Cobalt, and Nickel Complexes of Terdentate Ligands. *Inorg. Chem.* **1992**, *31*, 3680−3682.

(17) (a) Poater, A.; Ragone, F.; Giudice, S.; Costabile, C.; Dorta, R.; Nolan, S. P.; Cavallo, L. Thermodynamics of N-Heterocyclic Carbene Dimerization: The Balance of Sterics and Electronics. *Organometallics* **2008**, *27*, 2679−2681. (b) Poater, A.; Cosenza, B.; Correa, A.; Giudice, S.; Ragone, F.; Scarano, V.; Cavallo, L. SambVca: A Web Application for the Calculation of the Buried Volume of N-Heterocyclic Carbene Ligands. *Eur. J. Inorg. Chem.* **2009**, *2009*, 1759−1766.

(18) Chambers, J.; Eaves, B.; Parker, D.; Claxton, R.; Ray, P. S.; Slattery, S. J. Inductive influence of 4′-terpyridyl substituents on redox and spin state properties of iron(II) and cobalt(II) bis-terpyridyl complexes. *Inorg. Chim. Acta* **2006**, *359*, 2400−2406.

(19) Henderson, I. M.; Hayward, R. C. Substituent effects on the stabilities of polymeric and small molecule bis-terpyridine complexes. *Polym. Chem.* **2012**, *3*, 1221−1230.

DOI: 10.1021/acs.inorgchem.7b00595
Inorg. Chem. XXXX, XXX, XXX−XXX

(20) England, J.; Bill, E.; Weyhermuller, T.; Neese, F.; Atanasov, M.; Wieghardt, K. Molecular and Electronic Structures of Homoleptic Six-Coordinate Cobalt(I) Complexes of 2,2′:6′,2″-Terpyridine, 2,2′-Bipyridine, and 1,10-Phenanthroline. An Experimental and Computational Study. *Inorg. Chem.* **2015**, *54*, 12002−12018.
(21) Vargas, A.; Krivokapic, I.; Hauser, A.; Daku, L. M. L. Towards accurate estimates of the spin-state energetics of spin-crossover complexes within density functional theory: a comparative case study of cobalt(II) complexes. *Phys. Chem. Chem. Phys.* **2013**, *15*, 3752−3763.
(22) (a) Kilner, C. A.; Halcrow, M. A. An unusual discontinuity in the thermal spin transition in $[Co(terpy)_2][BF_4]_2$. *Dalton. Trans.* **2010**, *39*, 9008−9012. (b) Enachescu, C.; Krivokapic, I.; Zerara, M.; Real, J. A.; Amstutz, N.; Hauser, A. Optical investigation of spin-crossover in cobalt(II) bis-terpy complexes. *Inorg. Chim. Acta* **2007**, *360*, 3945−3950. (c) Kremer, S.; Henke, W.; Reinen, D. High-Spin−Low-Spin Equilibria of Cobalt(2+) in the Terpyridine Complexes $Co(terpy)_2X_2.nH_2O$. *Inorg. Chem.* **1982**, *21*, 3013−3022.
(23) *APEX 2, SAINT and SADABS*; Bruker AXS Inc., Madison, WI, USA, 2009.
(24) Sheldrick, G. M. *SHELXTL 2014/7*; University of Göttingen, Göttingen, Germany, 2014.
(25) Zhao, Y.; Truhlar, D. G. A new local density functional for main-group thermochemistry, transition metal bonding, thermochemical kinetics, and noncovalent interactions. *J. Chem. Phys.* **2006**, *125*, 194101−194118.
(26) (a) Mclean, A. D.; Chandler, G. S. Contracted Gaussian basis sets for molecular calculations. I. Second row atoms, Z = 11−18. *J. Chem. Phys.* **1980**, *72*, 5639−5648. (b) Krishnan, R.; Binkley, J. S.; Seeger, R.; Pople, J. A. Self-consistent molecular orbital methods. XX. A basis set for correlated wave functions. *J. Chem. Phys.* **1980**, *72*, 650−654.
(27) Frisch, M. J.; Trucks, G. W.; Schlegel, H. B.; Scuseria, G. E.; Robb, M. A.; Cheeseman, J. R.; Scalmani, G.; Barone, V.; Mennucci, B.; Petersson, G. A.; Nakatsuji, H.; Caricato, M.; Li, X.; Hratchian, H. P.; Izmaylov, A. F.; Bloino, J.; Zheng, G.; Sonnenberg, J. L.; Hada, M.; Ehara, M.; Toyota, K.; Fukuda, R.; Hasegawa, J.; Ishida, M.; Nakajima, T.; Honda, Y.; Kitao, O.; Nakai, H.; Vreven, T.; Montgomery, J. A., Jr.; Peralta, J. E.; Ogliaro, F.; Bearpark, M. J.; Heyd, J.; Brothers, E. N.; Kudin, K. N.; Staroverov, V. N.; Kobayashi, R.; Normand, J.; Raghavachari, K.; Rendell, A. P.; Burant, J. C.; Iyengar, S. S.; Tomasi, J.; Cossi, M.; Rega, N.; Millam, N. J.; Klene, M.; Knox, J. E.; Cross, J. B.; Bakken, V.; Adamo, C.; Jaramillo, J.; Gomperts, R.; Stratmann, R. E.; Yazyev, O.; Austin, A. J.; Cammi, R.; Pomelli, C.; Ochterski, J. W.; Martin, R. L.; Morokuma, K.; Zakrzewski, V. G.; Voth, G. A.; Salvador, P.; Dannenberg, J. J.; Dapprich, S.; Daniels, A. D.; Farkas, Ö.; Foresman, J. B.; Ortiz, J. V.; Cioslowski, J.; Fox, D. J. *Gaussian 09*; Gaussian, Inc., Wallingford, CT, USA, 2009.
(28) Dolg, M.; Wedig, U.; Stoll, H.; Preuss, H. Energy-adjusted ab initio pseudopotentials for the first row transition elements. *J. Chem. Phys.* **1987**, *86*, 866−872.

DOI: 10.1021/acs.inorgchem.7b00595
Inorg. Chem. XXXX, XXX, XXX−XXX